Article

Enhancement of Microwave Dielectric Properties in Mixed-Phase Ceramics Through CuB_2O_4 Doping: Achieving Ultra-Low Loss and High Dielectric Constant

Yuan-Bin Chen *, Siyi Xiong and Jie Peng *

School of Electronics and Electrical Engineering, Zhaoqing University, Zhaoqing 526061, China; xsy2471436141@163.com
* Correspondence: n2890103@outlook.com (Y.-B.C.); pengjie@zqu.edu.cn (J.P.)

Abstract: The microwave dielectric properties of $(1-x)Ca_{0.6}(La_{0.9}Y_{0.1})_{0.2667}TiO_3$-$x(Nd_{1/2}La_{1/2})$ $(Mg_{(1+\delta)1/2}Ti_{1/2})O_3$ ((1−x)CYTO-xNLMTO) ceramics were investigated in this study. It was discovered that the addition of 1 wt% CuB_2O_4 effectively enhanced the densification and improved the microwave dielectric properties of $(1-x)$CYTO-xNLMTO, where $\delta = 0.02$. The new ceramic systems of $(1-x)$CYTO-xNLMTO could achieve ultra-low loss and a high dielectric constant. The novel ceramic systems comprising $(1-x)$CYTO-xNLMTO exhibited remarkably low loss and a significantly high dielectric constant.

Keywords: ultra-low dielectric loss; $(1-x)Ca_{0.6}(La_{0.9}Y_{0.1})_{0.2667}TiO_3$-$x(Nd_{1/2}La_{1/2})(Mg_{(1+\delta)1/2}Ti_{1/2})O_3$; CuB_2O_4 doping; high dielectric constant

1. Introduction

With the rapidly increasing demands for 5G communication and satellite broadcasting, there is an urgent need to advance dielectric resonator materials in microwave frequency applications. The dielectric ceramics utilized in these applications must exhibit exceptional dielectric properties, including high permittivity (ε_r) [1–3], low dielectric loss (high Q × f) [4–8], and a temperature coefficient for the resonant frequency (τ_f) that approaches zero.

Designing high-quality devices is of paramount importance, with a focus on achieving optimal efficiency and stability while incorporating compact dimensions. Therefore, it is imperative to utilize dielectric materials with exceptional qualities for microwave resonators [9–11]. Specifically, the incorporation of high-k (ε_r) dielectric materials plays a crucial role in fabricating RF passive devices such as antenna filters and oscillator resonators, enabling reductions in resonator size. Furthermore, it is essential for these microwave materials to exhibit low-loss characteristics, leading to extensive research efforts aimed at developing dielectric materials with minimal microwave loss. The presence of this characteristic is essential for achieving high-frequency selectivity and stability in both microwave transmitters and receiver components. Ensuring near-zero temperature coefficients (τ_f) becomes imperative for maintaining stability across various operating temperatures in microwave components [12,13].

One promising approach involves utilizing two distinct ceramics with different τ_f values to form a solid solution or mixed phases, thereby effectively achieving a zero temperature coefficient of resonant frequency. This method addresses the demands of microwave circuit designs where precise control over each dielectric property is indispensable [14,15]. The dielectric ceramics utilized in microwave applications should consistently exhibit exceptional dielectric performance, encompassing a high permittivity (ε_r), low dielectric loss, and a near-zero temperature coefficient (τ_f) [16–18]. Perovskites, characterized by the general ABO_3 structure, have been extensively investigated for their application in

dielectric ceramics. They play a pivotal role in the fabrication of electronic components due to their high permittivity and reliability in practical scenarios [11,12].

Typically, the investigation of phase formation factors primarily involves considerations such as sintering temperature and thermal calculations [19,20], both of which have a significant impact on the manufacturing process cost [21]. To address this issue, extensive research efforts have been focused on minimizing sintering temperatures through various methods. Noteworthy approaches include the utilization of sol–gel processes, reduction in particle size, and liquid-phase sintering. The sol–gel process has emerged as a promising technique for reducing sintering temperatures by converting a solution or colloidal system into a gel, followed by drying and thermal treatment. This versatile route is known for producing high-purity materials with reduced processing temperatures. Another strategy involves decreasing the particle size of starting materials to enhance reactivity during sintering, thereby promoting densification at lower temperatures [22].

This approach not only contributes to energy efficiency but also mitigates the overall cost of the manufacturing process. Introducing a liquid phase by incorporating glass or other low-melting-point materials has proven effective in lowering the sintering temperature. Liquid-phase sintering facilitates the rearrangement of particles and enhances the diffusion process, leading to improved densification at reduced temperatures [23–26]. This method offers a practical solution for cost-effective manufacturing while maintaining the desired material properties.

After conducting a comprehensive literature review, it becomes evident that the sol–gel process is characterized by inherent complexity, while the alternative approach of reducing particle size in initial powders tends to increase fabrication costs [19,27–29]. Considering both cost efficiency and expedited fabrication as dual considerations, we have chosen to conduct experimental investigations utilizing liquid-phase sintering supplemented with the inclusion of other low-melting-point materials.

The compound $(Nd_{1/2}La_{1/2})(Mg_{1/2}Ti_{1/2})O_3$, referred to as NLMTO, possesses remarkable dielectric properties, characterized by a high dielectric constant ($\varepsilon_r \sim 27.6$), an impressive quality factor (Q $\times$ f value ~ 4550 GHz), and a negative temperature coefficient of resonant frequency (τ_f) of -48 ppm/°C. To counterbalance the positive τ_f value, the introduction of $Ca_{0.6}(La_{0.9}Y_{0.1})_{0.2667}TiO_3$, known as CYTO, with $\varepsilon_r = 111$, Q $\times$ f = 23,100 GHz, and $\tau_f = +374.6$ ppm/°C [30,31], into the composite system results in the formation of a solid solution, denoted as $(1-x)$CYTO-xNLMTO. In this investigation, CuB_2O_4 was selected as a sintering aid to effectively lower the sintering temperature of the $(1-x)$CYTO-xNLMTO ceramics. Moreover, the combination of NLMTO and CYTO yielded a novel dielectric system characterized by a high dielectric constant, a remarkable Q $\times$ f value, and a temperature coefficient of resonant frequency close to zero [32–34].

2. Experimental Procedure

The compositions CYTO and NLMTO were synthesized through mixed oxide solid-state reactions employing high-purity chemical powders, namely $CaCO_3$, TiO_2, La_2O_3, Nd_2O_3, Y_2O_3, TiO_2, and MgO. To address the hygroscopic nature of magnesium oxide, it underwent a drying process at 600 °C for 2 h. Stoichiometric ratios were maintained during the mixing of compositions, and the resulting mixture was ground in distilled water for 10 h using a baling mill with agate balls. Additionally, 1 wt% of the sintering aid $Cu-B_2O_3$ (CuB_2O_4) was introduced to $(1-x)$ CYTO-x NLMTO ceramics. Sintering of the ceramics was carried out at temperatures ranging from 1200 to 1350 °C for 4 h. Specifically, CYTO underwent calcination at 1000 °C for 2 h, while NLMTO was calcined at 1100 °C for 2 h. Polyvinyl alcohol (PVA 500; Showa, Tokyo, Japan), serving as a binder, was incorporated into the calcined powder. After achieving complete granulation uniformity, the mixture underwent screening with a 100-mesh screen and was pressed with a pressure of 200 MPa to form cylinders, each with a height of 0.5 cm and a diameter of 1.1 cm. Sintering temperatures (STs) for the cylinders were set at various temperatures for 4 h in an air environment, maintaining a consistent temperature rise and fall rate of 10 degrees

per minute across all specimens. Crystallization-phase observations of the pre-phased powder and the mixed compositions were conducted using a Siemens D5000 X-Ray Powder diffractometer (XRD, Munich, Germany) with Cu-Kα radiation (at 40 kV and 40 mA). The XRD analysis of the sample was executed at a scan speed of 2 degrees/minute and a step size of 0.06 degrees. Utilizing Scanning Electron Microscopy (SEM, SEM4000Pro, ZEISS, Oberkochen, Germany) technology, the grain size, shape, and distribution of the sample were meticulously observed. Meanwhile, through the application of Energy Dispersive Spectroscopy (EDS) analysis, the types and concentrations of elements contained within the sample were determined. Bulk densities of the sintered pellets were determined using the Archimedes method. Measurements of ε_r and Q × f at radio frequencies were carried out using the Hakki–Coleman [35] dielectric resonator method, employing a network analyzer (Anritsu MS4647B, Morgan Hill, CA, USA). The same technique was utilized to measure the temperature coefficient of resonant frequency (τ_f). The test set was subjected to a thermostat-controlled environment in a temperature range from +25 °C to +80 °C. Additionally, the temperature coefficient of resonant frequency (τ_f) was calculated using Equation (1).

$$\tau_f = \frac{f_{t2} - f_{t1}}{(t_2 - t_1)f_{t1}} \times 10^6 \ (\text{ppm}/°\text{C}) \tag{1}$$

In the above equation, f_{t2} and f_{t1} represent the resonant frequencies at 80 °C and 25 °C, respectively.

3. Results and Discussion

The XRD analyses were performed after incorporating 1 wt% of multiple sintering aids, specifically CuO-B_2O_3 (CuB_2O_4), into the $(1-x)$CYTO-xNLMTO ceramics. These ceramics were sintered at temperatures ranging from 1200 to 1325 °C for a duration of 4 h. Due to the close resemblance in lattice parameters between the two ceramics, a solid solution was formed. Figure 1 shows peaks that confirm the presence of NLMTO and CYTO as crystalline phases in the composition of 0.15CYTO-0.85NLMTO. All identified peaks were successfully indexed based on the perovskite structure, with no evidence of a second phase observed across all compositions examined in this experiment.
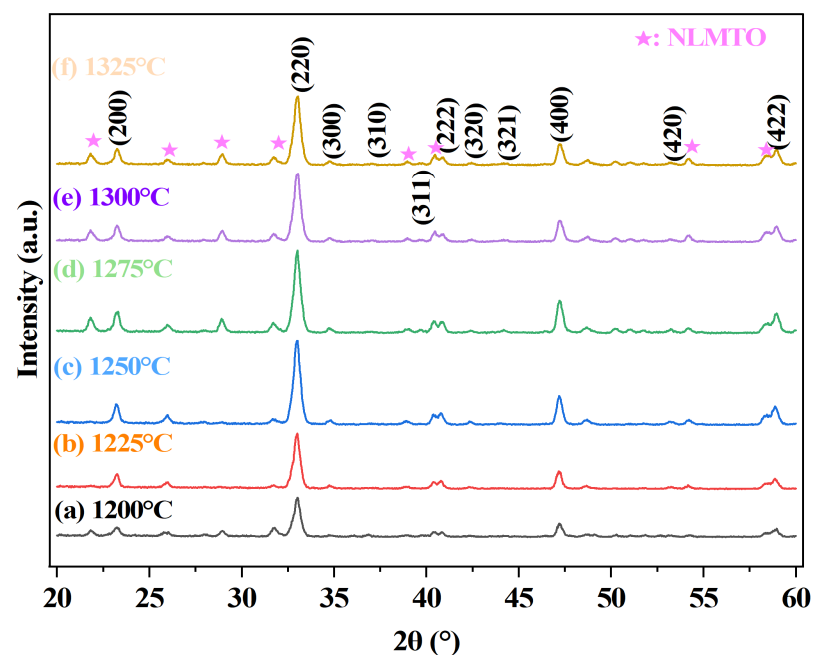

Figure 1. X-ray diffraction patterns of the $0.15Ca_{0.6}(La_{0.9}Y_{0.1})_{0.2667}TiO_3$-$0.85(Nd_{1/2}La_{1/2})$ $(Mg_{(1+\delta)1/2}Ti_{1/2})O_3$ system with 1 wt% CuB_2O_4 additive sintered at various temperatures: (**a**) 1200 °C; (**b**) 1225 °C; (**c**) 1250 °C; (**d**) 1275 °C; (**e**) 1300 °C; (**f**) 1325 °C for 4 h.

The SEM results for the 0.15CYTO-0.85NLMTO ceramics with single additives in varying amounts, sintered at temperatures ranging from 1200 to 1325 °C for a duration of four hours, are presented in Figure 2. The density of the ceramics exhibits an increasing trend with higher sintering temperatures, reaching its peak value at 1250 °C due to enhanced particle mobility and optimal packing efficiency. However, further elevation of temperature can lead to detrimental effects such as excessive crystal growth, grain coarsening, and defect formation. The findings obtained from EDS, as depicted in Figure 2c with labeled spots A–D, have been meticulously documented in Table 1. These spots (A–D) correspond to grains exhibiting distinct classifications: spot A represents large cubic structures; spot B displays polygonal morphology; while spots C and D exhibit smaller rounded shapes. Importantly, the atomic percentages determined through analysis of spots A–D closely align with the expected ratio of 0.15CYTO-0.85NLMTO composition. These outcomes are consistent with those obtained from XRD analysis and affirm the absence of any discernible formation of secondary phases.
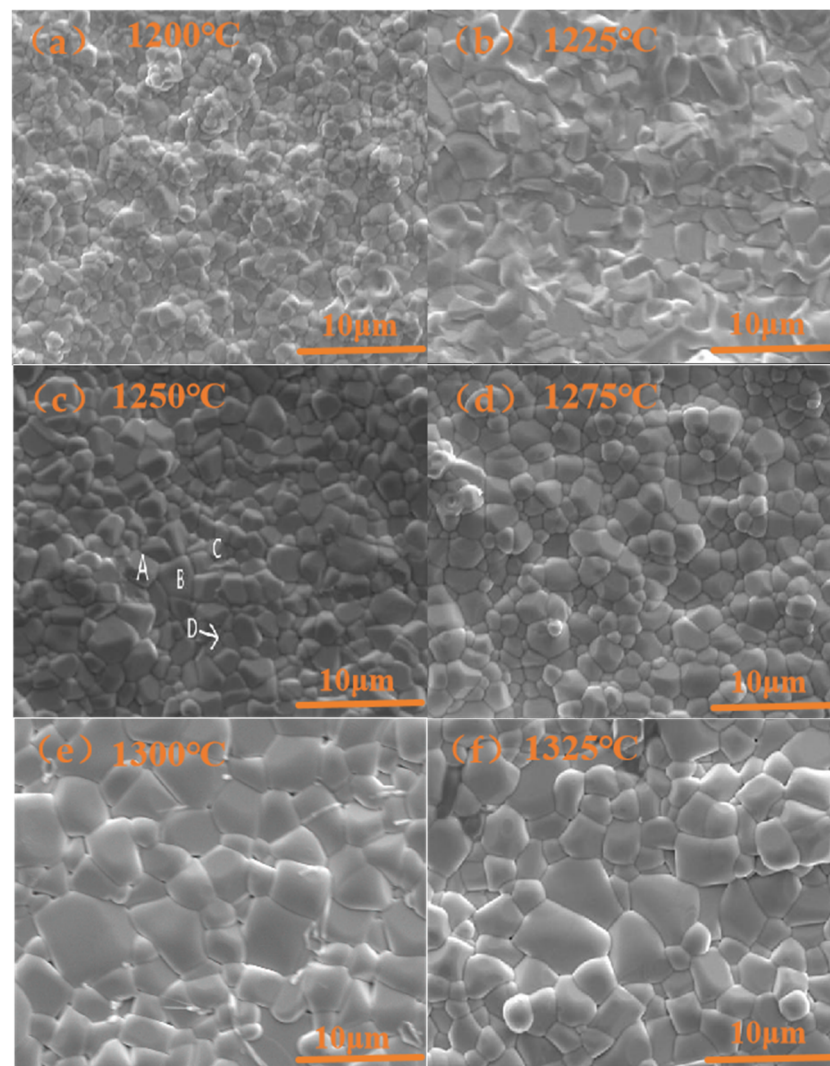

Figure 2. SEM photographs of $0.15Ca_{0.6}(La_{0.9}Y_{0.1})_{0.2667}TiO_3$-$0.85(Nd_{1/2}La_{1/2})(Mg_{(1+\delta)1/2}Ti_{1/2})O_3$ ceramics with 1 wt% CuB_2O_4 additive sintered at (**a**) 1200 °C; (**b**) 1225 °C; (**c**) 1250 °C; (**d**) 1275 °C; (**e**) 1300 °C; (**f**) 1325 °C.

Figure 3 displays the variation in relative density of the (1−x)CYTO-x NLMTO ceramics as a function of sintering temperature and the parameter x. Ceramics with different x values exhibit a similar trend in response to temperature changes. The relative den-

sity of the samples peaks at 1250 °C, highlighting a critical temperature where optimal densification is achieved across all compositions. When x = 0.85, the observed relative density reaches an impressive 95%, with an apparent density of 5.85 g/cm^3, indicating an exceptionally robust crystal structure. Such a high relative density suggests effective packing and arrangement of particles, which positively contributes to the integrity and quality of the crystal lattice. Additives of 1 wt% CuB_2O_4 were introduced into the sintering process. It serves a multi-faceted role in influencing the material's properties during the sintering phase. By lowering the material's melting point, it instigates the creation of a liquid phase amid sintering, which leads to the enhancement of particle mobility and the formation of larger crystal grains upon solidification [26]. Furthermore, CuB_2O_4 actively promotes the bonding of adjacent particles throughout the sintering process, which results in the development of a more interconnected and denser structure. Additionally, CuB_2O_4 facilitates the diffusion of atoms within the powder particles, improving atomic mobility. This augmented diffusion process further stimulates the rearrangement of atoms during sintering, ultimately fostering the growth of larger crystal grains. Moreover, the CuB_2O_4 additives may play a crucial role in reducing the surface energy of the particles. This reduction in surface energy facilitates the convergence of particles, making it easier for them to come together and form larger grains. The lower surface energy actively encourages particles to merge and coalesce during the sintering process.

Table 1. EDS analysis results for $(1-x)Ca_{0.6}(La_{0.9}Y_{0.1})_{0.2667}TiO_3\text{-}x(Nd_{1/2}La_{1/2})(Mg_{(1+\delta)1/2}Ti_{1/2})O_3$ ceramics with x = 0.85 sintered at 1250 °C.

Spot	Element Atomic (%)						
	Ca	**La**	**Y**	**Ti**	**O**	**Nd**	**Mg**
A	10.2	5.5	0.45	18.5	60	1.5	3.85
B	9.8	4.9	0.61	17.1	61.74	1.91	3.94
C	9.9	5.2	0.49	16.2	62.93	1.45	3.83
D	10.1	6	0.48	15.3	62.63	1.39	4.1
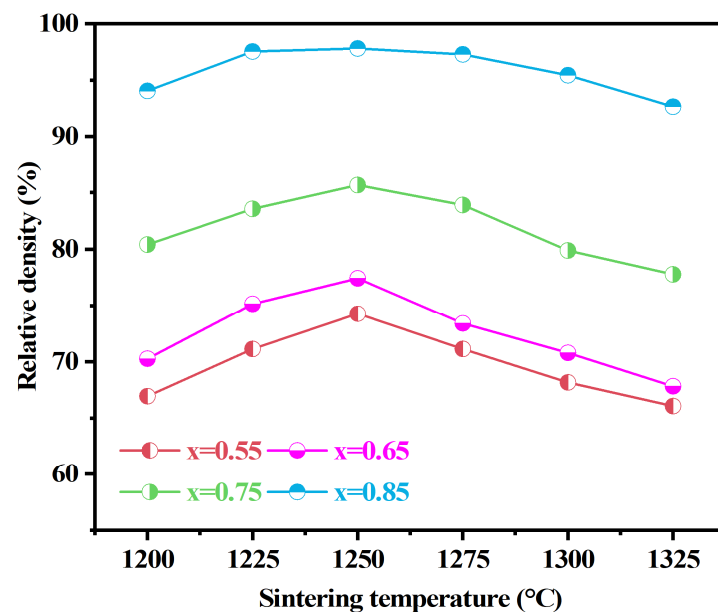
Figure 3. Relative density of $(1\text{-}x)Ca_{0.6}(La_{0.9}Y_{0.1})_{0.2667}TiO_3\text{-}x(Nd_{1/2}La_{1/2})(Mg_{(1+\delta)1/2}Ti_{1/2})O_3$ ceramics with 1 wt% CuB_2O_4 additive system sintered at various temperatures for 4 h.

The dielectric constants of the $(1-x)$CYTO-xNLMTO ceramics, with 1 wt% CuB_2O_4 additives, sintered at various temperatures for 4 h and considering different x values, are presented in Figure 4. ε_r and densities consistently exhibit parallel trends across the range

of sintering temperatures. Ceramics with higher density show elevated ε_r due to reduced pore presence, thereby mitigating decay effects. Specifically, the ε_r value for the 0.15CYTO-0.85NLMTO ceramics reaches saturation around 35 when sintered at a temperature of 1250 °C for 4 h. The dielectric constants of CYTO and NLMTO were measured as 111 and 27.6, respectively [32,33]. Notably, there is a decreasing trend in ε_r with increasing x value attributed to lower dielectric constants observed in NLMTO ceramics; specifically, the dielectric constants decrease from 48.52 ± 0.13 to 35.01 ± 0.14 as x values increase from 0.55 to 0.85, respectively. This observed relationship aligns with the trends seen in densities and sintering temperatures, where a higher density corresponds to lower porosity levels. The interplay between ε_r values and sintering temperatures underscores the intricate connection between material composition, porosity, and dielectric properties exhibited by these ceramics.
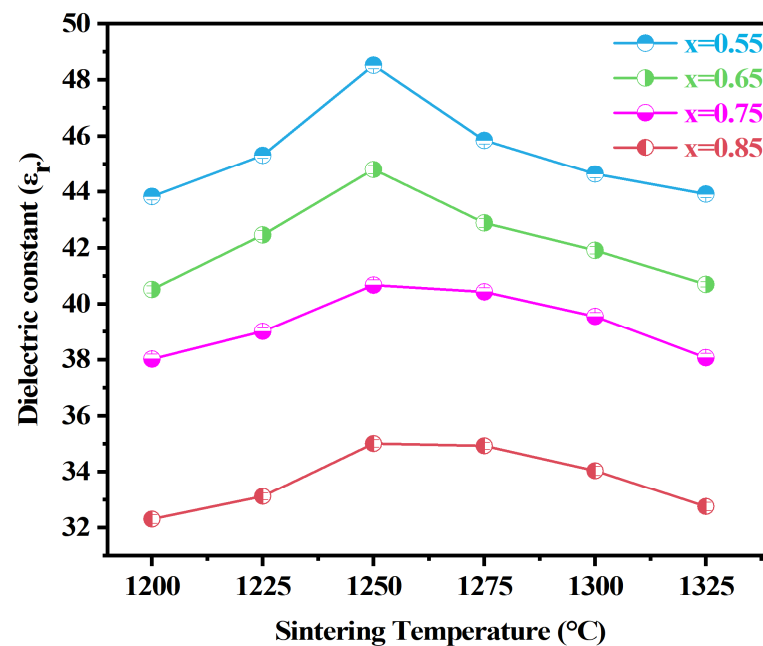

Figure 4. Dielectric constant of the $(1-x)Ca_{0.6}(La_{0.9}Y_{0.1})_{0.2667}TiO_3-x(Nd_{1/2}La_{1/2})(Mg_{(1+\delta)1/2}Ti_{1/2})O_3$ ceramics with 1 wt% CuB_2O_4 additive sintered at various temperatures for 4 h.

The correlation between sintering temperature and the value of Q × f for different x values is depicted in Figure 5. As expected, the Q × f value exhibits an increase with the augmentation of NLMTO content, owing to its significantly higher quality factor compared to CYTO. Several factors can influence microwave dielectric loss in dielectric resonators, including lattice vibrational modes, pores, and secondary phases. Generally, a larger grain size and smaller grain boundaries indicate reduced lattice imperfections leading to decreased dielectric loss. Evidence supports the claim that phase transformation primarily governs the dielectric loss in the $(1-x)CYTO-xNLMTO$ ceramics system.

Figure 6 illustrates the temperature coefficients of τ_f for the $(1-x)CYTO-xNLMTO$ ceramics. Specifically, a τ_f value of 12.06 ± 0.6 ppm/°C was achieved for 0.15CYTO-0.85NLMTO ceramics that contained 1 wt% CuB2O4 additive and were sintered at 1250 °C for 4 h. It is widely acknowledged that τ_f is influenced by various factors, including composition, additives, and the presence of secondary phases within the material. Generally, a higher CYTO content tends to result in a more positive τ_f value.

Figure 7 showcases the simulation results for the band-pass filter utilizing a substrate made of 0.15CYTO-0.85NLMTO ceramic material. The experimental implementation of the band-pass filter using the same ceramic substrate is presented in Figure 8. Detailed simulation results can be found in Table 2, whereas Table 3 outlines the performance characteristics of the filter employing the 0.15CYTO-0.85NLMTO ceramic substrate when

compared to FR4 and Al_2O_3 substrates. The differences between Figure 7 (Simulation results) and Figure 8 (Measurement results) stem from the fact that the actual fabricated substrate has gaps on its surface, and the printed conductive metal material surface is not absolutely flat. Additionally, the simulation parameters do not account for the loss of surface metal, nor do they include the loss parameters of SMA connectors. Therefore, there will be slight differences between the simulation results and actual measurements. Notably, this design approach leverages an electromagnetic (EM) simulator like IE3D to accurately determine the physical dimensions of the filter.
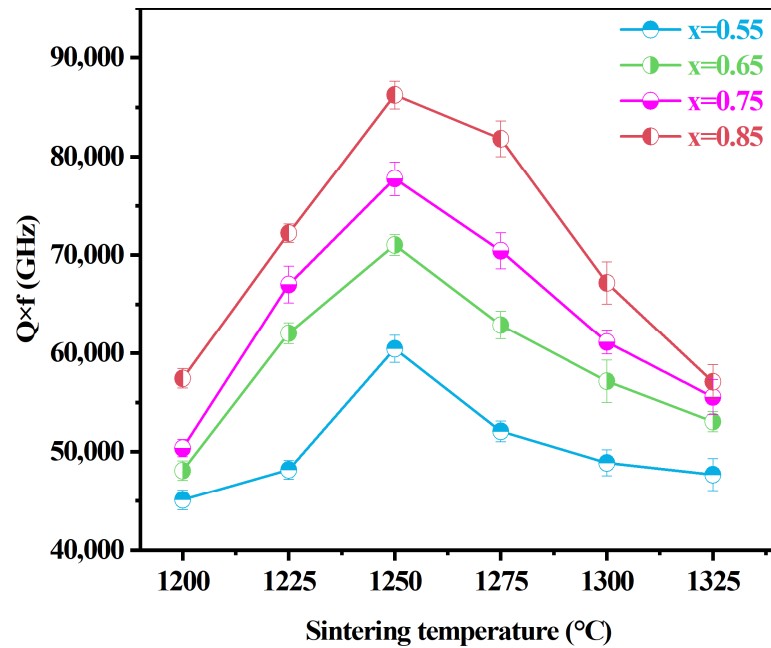

Figure 5. $Q \times f$ value of $(1-x)Ca_{0.6}(La_{0.9}Y_{0.1})_{0.2667}TiO_3$-$x(Nd_{1/2}La_{1/2})(Mg_{(1+\delta)1/2}Ti_{1/2})O_3$ ceramics with 1 wt% CuB_2O_4 additive system sintered at various temperatures for 4 h.

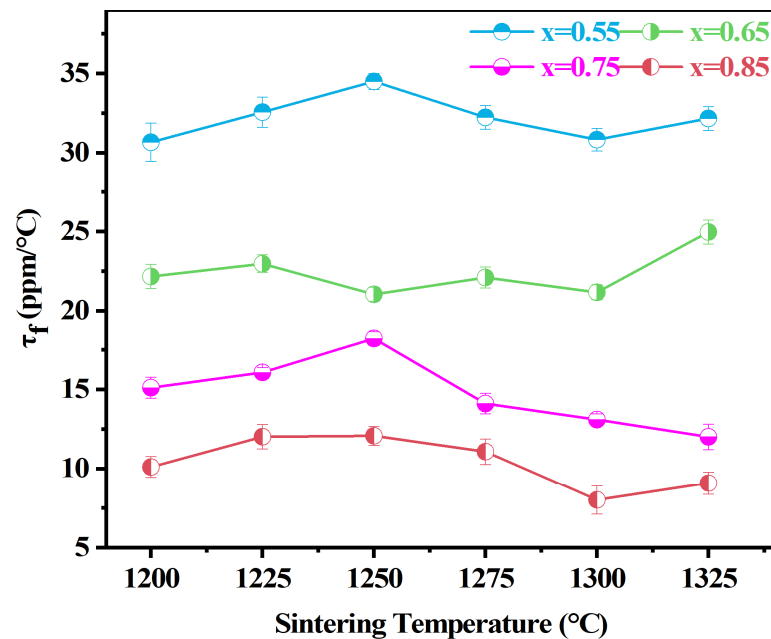**Figure 6.** Temperature coefficient of the resonant frequency of $(1-x)Ca_{0.6}(La_{0.9}Y_{0.1})_{0.2667}TiO_3$-$x(Nd_{1/2}La_{1/2})(Mg_{(1+\delta)1/2}Ti_{1/2})O_3$ ceramics with 1 wt% CuB_2O_4 additive sintered at various temperatures for 4 h.
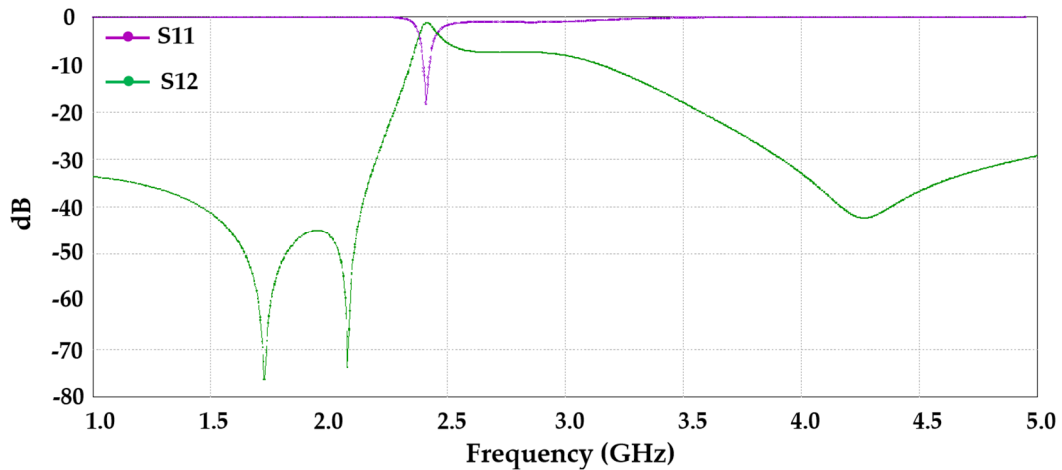
Figure 7. The simulation band-pass filter with $0.15Ca_{0.6}(La_{0.9}Y_{0.1})_{0.2667}TiO_3$–$0.85(Nd_{1/2}La_{1/2})$ $(Mg_{(1+\delta)1/2}Ti_{1/2})O_3$ ceramic substrate (S11: Reflection Loss, S21:Insertion Loss).
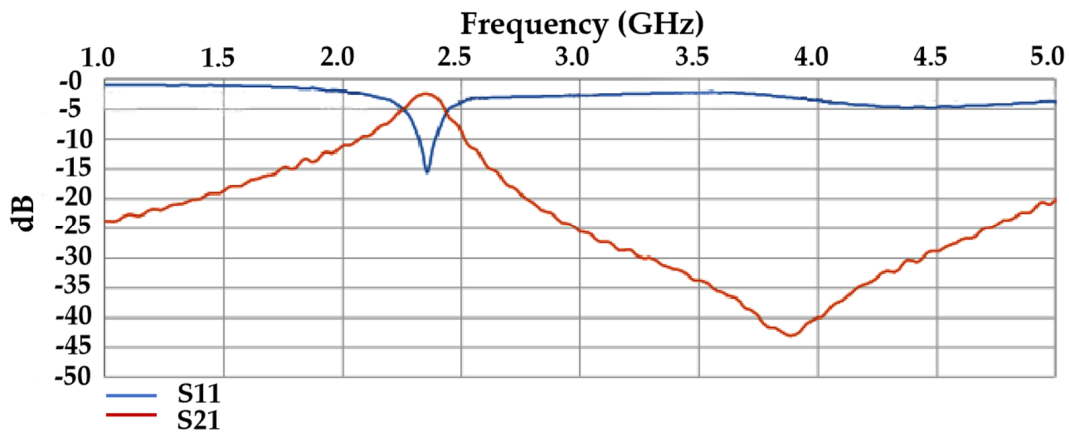

Figure 8. The measured band-pass filter with $0.15Ca_{0.6}(La_{0.9}Y_{0.1})_{0.2667}TiO_3$–$0.85(Nd_{1/2}La_{1/2})$ $(Mg_{(1+\delta)1/2}Ti_{1/2})O_3$ ceramic substrate (S11: Reflection Loss, S21:Insertion Loss).

Table 2. Simulation results of the band-pass filters with various dielectrics.

Substrate	tanδ	ε_r	Size (mm^2)	Insertion Loss (dB)	Return Loss (dB)	f_o (GHz)
FR4	0.015	4.5	24×64	2.5	23.9	2.4
Al$_2$O$_3$	0.003	9.8	15×42	1.5	21	2.4
0.15CLYT-0.85LNMT	0.0001	35	7.51×9.5	0.7	21.1	2.4

Table 3. The performance filter with $(1-x)Ca_{0.6}(La_{0.9}Y_{0.1})_{0.2667}TiO_3$-$x(Nd_{1/2}La_{1/2})(Mg_{(1+\delta)1/2}Ti_{1/2})O_3$ ceramic substrate.

		f_0 (GHz)	S_{11} (dB)	S_{21} (dB)	Bandwidth (%)	Size (mm^2)
0.15CLYT-0.85LNMT	simulation	2.4	-19.44	-0.37	10.1%	7.51×9.5
	measured	2.4	-15.24	-1.69	10.3%	

4. Conclusions

The dielectric characteristics of $(1-x)$CLYO-xNLMTO ceramics incorporating CuB$_2$O$_4$ sintering aids were systematically investigated in this study. The resulting ceramics exhibited distinct perovskite structures. A non-linear variation in Q $\times$ f was observed, indicating an increasing trend for compositions with x $\geq$ 0.5. Notably, the 0.15CLYO-0.85NLMTO

composition, sintered at 1250 °C for 4 h, demonstrated exceptional dielectric properties including a dielectric constant of 35 and a Q × f value reaching 81,900 GHz. Moreover, it displayed a favorable τ_f at 15 ppm/°C. These findings highlight the promising potential of these ceramics for applications requiring high-performance dielectric materials.

Author Contributions: Methodology, J.P.; formal analysis, Y.-B.C.; investigation, S.X.; data curation, Y.-B.C.; project administration, J.P.; funding acquisition, S.X. All authors have read and agreed to the published version of the manuscript.

Institutional Review Board Statement: Not applicable.

Informed Consent Statement: Not applicable.

Data Availability Statement: The original contributions presented in this study are included in the article; further inquiries can be directed to the corresponding author(s).

Conflicts of Interest: The authors declare that they have no known competing financial interests or personal relationships that could have appeared to influence the work reported in this paper.

References

1. Zhang, P.; Hao, M.; Xiao, M. Microwave dielectric properties of $Li_3Mg_2NbO_6$-based ceramics with $(M_xW_{1-x})^{5+}$ (M = Li^+, Mg^{2+}, Al^{3+}, Ti^{4+}) substitutions at Nb^{5+} sites. *J. Alloys Compd.* **2021**, *853*, 157386. [CrossRef]
2. Nakagoshi, Y.; Sato, J.; Morimoto, M.; Suzuki, Y. Near-zero volume-shrinkage in reactive sintering of porous $MgTi_2O_5$ with pseudobrookite-type structure. *Ceram. Int.* **2016**, *42*, 9139–9144. [CrossRef]
3. Lin, S.H.; Chen, Y.B. Structure and characterization of B_2O_3 modiffed $yNd(Mg_{1/2}Ti_{1/2})O_3$-$(1-y)Ca_{0.8}Sr_{0.2}TiO_3$ ceramics with a near-zero temperature coefffcient at microwave frequency. *Ceram. Int.* **2017**, *43*, 2368–2371. [CrossRef]
4. Zaman, A.; Uddin, S.; Mehboob, N.; Ali, A. Structural investigation and improvement of microwave dielectric properties in $Ca(Hf_xTi_{1-x})O_3$ ceramics. *Phys. Scr.* **2021**, *96*, 025701. [CrossRef]
5. Wang, K.; Zhou, H.; Luan, X.; Hu, S.; Zhou, X.; He, S.; Wang, X.; Zhou, S.; Chen, X. $NaTaO_3$ microwave dielectric ceramic a with high relative permittivity and as an excellent compensator for the temperature coefffcient of resonant frequency. *Ceram. Int.* **2021**, *47*, 121–129. [CrossRef]
6. Pei, C.; Tan, J.; Li, Y.; Yao, G.; Jia, Y.; Ren, Z.; Liu, P.; Zhang, H. Effect of Sb-site nonstoichiometry on the structure and microwave dielectric properties of $Li_3Mg_2Sb_{1-x}O_6$ ceramics. *J. Adv. Ceram.* **2020**, *9*, 588–594. [CrossRef]
7. Chen, C.; Peng, Z.; Xie, L.; Bi, K.; Fu, X. Microwave dielectric properties of novel $(1 - x)MgTiO_3 - xCa_{0.5}Sr_{0.5}TiO_3$ ceramics. *J. Mater. Sci. Mater. Electron.* **2020**, *31*, 13696–13703. [CrossRef]
8. Li, J.; Zhang, C.; Liu, H.; Qiu, T.; Fan, C. Structure, morphology, and microwave dielectric properties of $SmAlO_3$ synthesized by stearic acid route. *J. Adv. Ceram.* **2020**, *9*, 558–566. [CrossRef]
9. Hameed, X.; Liu, Q.; Li, L.; Liu, M.Y.; Chen, X.M. Structure evolution and improved microwave dielectric characteristics in $CaTi_{1-x}(Al_{0.5}Nb_{0.5})xO_3$ ceramics. *J. Alloys Compd.* **2020**, *845*, 155435. [CrossRef]
10. Wu, M.; Zhang, Y.; Xiang, M. Synthesis, characterization and dielectric properties of a novel temperature stable $(1-x)CoTiNb_2O_{8-x}ZnNb_2O_6$ ceramic. *J. Adv. Ceram.* **2019**, *8*, 228–237. [CrossRef]
11. Shi, F.; Fu, G.; Xiao, E.; Li, J. Lattice vibrational characteristics and dielectric properties of pure phase $CaTiO_3$ ceramic. *J. Mater. Sci. Mater. Electron.* **2020**, *31*, 18070–18076. [CrossRef]
12. Yang, S.; Liang, B.; Liu, C.; Liu, J.; Fang, C.; Ai, Y. Microwave sintering and microwave dielectric properties of $(1-x)Ca_{0.61}La_{0.26}TiO_3 - xNd(Mg_{0.5}Ti_{0.5})O_3$ ceramics. *Materials* **2021**, *14*, 438. [CrossRef] [PubMed]
13. Takahashi, H.; Baba, Y.; Ezaki, K.; Okamoto, Y.; Shibaba, K.; Kuroki, K.; Nakano, S. Dielectric characteristics of $(A^{1+}_{0.5}A^{3+}_{0.5})TiO_3$ ceramics at microwave frequencies. *Jpn. J. Appl. Phys.* **1991**, *30*, 2339–2342. [CrossRef]
14. Mercurio, J.P.; Manier, M.; Frit, B. Dielectric properties of ceramics within the $BaOLn_2O_3$-TiO_2 system. *Ferroelectrics* **1992**, *127*, 35–40. [CrossRef]
15. Ezaki, K.; Baba, Y.; Takahashi, H.; Shibata, K.; Nakano, S. Microwave dielectric properties of CaO-Li_2O-Ln_2O_3-TiO_2 ceramics. *Jpn. J. Appl. Phys.* **1993**, *1*, 4319–4322. [CrossRef]
16. Kato, J.; Kagata, H.; Nishimoto, K. Dielectric properties of lead alkaline-earth zirconate at microwave frequencies. *Jpn. J. Appl. Phys.* **1991**, *30*, 2343–2346. [CrossRef]
17. Yan, Y.; Li, Z.; Zhang, M.; Sun, P.; Xu, Y. Preparation and microwave dielectric properties of $Ca_{0.6}La_{0.8/3}(Sn_xTi_{1-x})O_3$ ceramics. *Ceram. Int.* **2017**, *43*, 8534–8537. [CrossRef]

18. Wise, P.L.; Reaney, I.M.; Lee, W.E.; Price, T.J.; Iddles, D.M.; Cannell, D.S. Structure–microwave property relations in $(Sr_xCa_{(1-x)})_{n+1}Ti_nO_{3n+1}$. *J. Eur. Ceram. Soc.* **2001**, *21*, 1723–1726. [CrossRef]
19. Takada, T.; Wang, S.F.; Yoshikawa, S.; Jang, S.-J.; Newnham, R.E. Effect of Glass Additions on BaO-TiO₂-WO₃ Microwave Ceramics. *J. Am. Ceram. Soc.* **1994**, *77*, 1909–1916. [CrossRef]
20. Takada, T.; Wang, S.F.; Yoshikawa, S.; Jang, S.-J.; Newnham, R.E. Effects of glass additions on (Zr, Sn) TiO₄ for microwave applications. *J. Am. Ceram. Soc.* **1994**, *77*, 2485–2488. [CrossRef]
21. Hirno, S.; Hayashi, T.; Hattori, A. Chemical Processing and Microwave Characteristics of (Zr,Sn)TiO₄ Microwave Dielectrics. *J. Am. Ceram. Soc.* **1991**, *74*, 1320–1324. [CrossRef]
22. Tolmer, V.; Desgardin, G. Low-temperature sintering and influence of the process on the dielectric properties of Ba $(Zn_{1/3}Ta_{2/3})$ O₃. *J. Am. Ceram. Soc.* **1997**, *80*, 1981. [CrossRef]
23. Choy, J.H.; Han, Y.S. Microwave characteristics of BaO–TiO₂ ceramics prepared via a citrate route. *J. Am. Ceram. Soc.* **1995**, *78*, 1167–1172. [CrossRef]
24. Weng, M.H.; Liang, T.J.; Huang, C.L. Lowering of sintering temperature and microwave dielectric properties of BaTi₄O₉ ceramics prepared by the polymeric precursor method. *J. Eur. Ceram. Soc.* **2002**, *22*, 1693–1698. [CrossRef]
25. Yang, C.F. The microwave characteristics of glass-BaTi₄O₉ ceramics. *Jpn. J. Appl. Phys.* **1999**, *38*, 3576–3579. [CrossRef]
26. Yang, J.; Huang, M.; Wang, F.; Zhu, K.; Yan, K. Low temperature sintering, structure and electrical properties of BiFeO₃-BaTiO₃ based piezoelectric ceramics using CuO-B₂O₃ composite sintering aids. *Mater. Sci. Eng. B* **2023**, *298*, 116872. [CrossRef]
27. Kim, D.W.; Lee, D.G.; Hong, K.S. Low-temperature firing and microwave dielectric properties of BaTi₄O₉ with Zn–B–O glass system. *Mater. Res. Bull.* **2001**, *36*, 585–595. [CrossRef]
28. Lu, S.G.; Kwok, K.W.; Chan, H.L.; Choy, C.L. Structural and electrical properties of BaTi₄O₉ microwave ceramics incorporated with glass phase. *Mater. Sci. Eng.* **2003**, *B99*, 491–494. [CrossRef]
29. Cheng, C.M.; Yang, C.F.; Lo, S.H.; Tseng, T.Y. Sintering BaTi₄O₉/Ba₂Ti₉O₂₀-based ceramics by glass addition. *J. Eur. Ceram. Soc.* **2000**, *20*, 1061–1067. [CrossRef]
30. Seabra, M.P.; Salak, A.N.; Avdeev, M.; Ferreira, V.M. Structure and dielectric characterization of the La(Mg₁/₂Ti₁/₂)O₃-Nd(Mg₁/₂Ti₁/₂)O₃ system. *J. Phys. Condens. Matter* **2003**, *15*, 4229. [CrossRef]
31. Lin, S.-H.; Lin, Z.-Q.; Chen, C.-W. Microwave dielectric characterization of $Ca_{0.6}(La_{1-x}Y_x)_{0.2667}TiO_3$ perovskite ceramics with high positive temperature coefficient. *Ceram. Int.* **2021**, *47*, 16828–16832. [CrossRef]
32. Jhou, M.Z.; Jean, J.H. Low-fire processing of microwave BaTi4O9 with BaO–ZnO–B₂O₃ glass. *J. Am. Ceram. Soc.* **2006**, *89*, 786–791. [CrossRef]
33. Lim, J.B.; Kim, M.H.; Kim, J.C.; Nahm, S.; Paik, J.H.; Kim, J.H. Effect of BaCuB₂O₅ additive on the sintering temperature and microwave dielectric properties of BaTi₄O₉ ceramics. *Jpn. J. Appl. Phys.* **2006**, *45*, 242–244. [CrossRef]
34. Choi, Y.J.; Park, J.H.; Ko, W.J.; Park, J.H.; Nahm, S.; Park, J.G. Low temperature sintering of BaTi₄O₉-based middle-k dielectric composition for LTCC applications. *J. Electroceramics* **2005**, *14*, 157–162. [CrossRef]
35. Hakki, B.W.; Coleman, P.D. A dielectric resonator method of measuring inductive capacities in the millimeter range. *IEEE Trans. Microw. Theory Tech.* **1960**, *8*, 402–410. [CrossRef]